Optogenetic Control of RhoA Reveals Zyxin-mediated Elasticity of Stress Fibers

Patrick W. Oakes[1,4*^], Elizabeth Wagner[2*], Christoph A. Brand[3+], Dimitri Probst[3+], Marco Linke[3+], Ulrich S. Schwarz[3^], Michael Glotzer[2^], Margaret L. Gardel[1^]

[1]Institute for Biophysical Dynamics, James Franck Institute and the Department of Physics, University of Chicago, Chicago, IL 606037

[2]Department of Molecular Genetics and Cell Biology, University of Chicago, Chicago, IL 60637

[3]Institute for Theoretical Physics and BioQuant, Heidelberg University, Heidelberg, Germany

[4]Department of Physics & Astronomy, and Department of Biology, University of Rochester, Rochester, NY 14627

[*,+]Contributed equally

[^]Corresponding Authors

Abstract

The mechanics of the actin cytoskeleton regulates cell morphogenesis during essential physiological processes. While cellular contractility is known to be largely RhoA-dependent, the process by which localized biochemical signals are translated into cell-level responses is not well understood. Here we combine optogenetic control of RhoA in space and time, live cell imaging and traction force microscopy to investigate the dynamics of actomyosin-based force generation in adherent fibroblasts. Local activation of RhoA not only stimulates local recruitment of actin and myosin, but also leads to increased traction forces outside the activation region that rapidly propagate across the cell via stress fibers and drive actin flow towards the region of heightened RhoA. Surprisingly, the flow reverses direction when local RhoA activation stops. We identify zyxin as a regulator of stress fiber mechanics, as stress fibers are fluid-like without flow reversal in its absence. These experimental data are used to constrain a physical model, which demonstrates that stress fibers are elastic-like, even at time scales exceeding turnover of constituent proteins. Such molecular control of actin mechanics likely plays critical roles in regulation of morphogenic events.

Introduction

A diverse array of essential physiological processes, ranging from the subcellular to the multicellular, depend on the spatial and temporal regulation of contractile forces[1-4]. This regulation drives changes in cell shape[5,6] and mediates interactions with the extracellular environment [7,8]. Changes in contractility can furthermore alter gene expression[9] and impact development[10,11]. The molecular machinery required for generating contractile forces is well conserved and dominated by the actin cytoskeleton, myosin II activity and associated regulatory proteins[4,12,13]. Specifically, actin filaments dynamically organize into distinct contractile architectures, including the cortex and stress fibers [14,15]. Contractile forces are transmitted across the cell by actin arrays and ultimately to the extracellular matrix by focal adhesions[12,13,16,17].

The regulation of cellular force transmission is controlled by the mechanical properties of actomyosin assemblies. Cellular mechanics has been explored extensively both experimentally[14,18-20] and theoretically[21-23]. The current understanding is that, at time scales up to those of typical kinetic

processes, the actin cytoskeleton behaves like an elastic solid. Such elasticity enables rapid force transmission across the cell and reversible deformations to preserve cytoskeletal architecture. In contrast, at longer time scales, it is thought that dynamic processes make the cytoskeleton predominately like a viscous fluid, enabling cytoskeletal flows and remodeling. These dynamic processes including exchange of proteins from the cytosol and are typically on the order of tens of seconds in structures like the cortex[24,25] and on the order of a minute in stress fibers[26]. The molecular regulation underlying the competition between elastic and viscous processes in cells is not well understood.

Cellular contractility is largely controlled by the activity of the small GTPase RhoA[27,28], which in adherent cells is preferentially active at the cell periphery[29,30]. RhoA regulates contractility through the promotion of actin polymerization and myosin light chain phosphorylation via the downstream effectors Diaphanous-related formins and Rho-associated Kinase (ROCK), respectively. RhoA activity is required for stress fibers and focal adhesions[27,28]. Little, however, is known about how small changes in activity can regulate cell contractility, actin architecture and adhesion.

Optogenetics has been used before to control cell migration and cell forces[31-34]. Here we have used an optogenetic probe to locally activate RhoA in adherent fibroblasts. Plasma membrane recruitment of the RhoA specific guanine exchange factor (GEF) LARG induces local RhoA activation[6,35-37]. Local activation of RhoA leads to an increase in actin polymerization and myosin activity in the region of activation, but it does not stimulate *de novo* stress fiber formation or changes in focal adhesion morphology. We find that exogenous RhoA activation leads to an immediate increase in both the local and global contractility of the cell, followed by a rapid relaxation after GEF recruitment is stopped. The local increase in stress fiber contractility drives an actomyosin flow towards regions of increased RhoA activity. Surprisingly, these flows reverse direction as soon as GEF recruitment ceases. Using physical modeling, we show this behavior is consistent with stress fibers behaving as predominately elastic-like over time scales much longer than minutes. We find that zyxin is necessary for this elasticity; in its absence, stress fibers become predominately fluid-like even at second time scales. These results

suggest that stress fiber mechanics is sensitive to small changes in composition, which has significant implications for regulation of force transmission and cytoskeletal organization.

Results

Spatiotemporal control of RhoA and its downstream effectors

To spatially and temporally control contractility in adherent cells, we adapted a previously established optogenetic probe[6,35] to act on the RhoA signaling pathway (Figure 1a). During stimulation by blue light, a cytosolic fusion protein, photo-recruitable GEF (prGEF), consisting of tandem PDZ domains fused to the DH domain of the RhoA specific GEF LARG[6], is recruited to the plasma membrane where it activates RhoA (Figure 1b). To illustrate the local recruitment of prGEF we tagged it with the fluorophore mCherry and imaged an NIH 3T3 fibroblast expressing the constructs on a glass coverslip (Figure 1c). A digital micromirror device was used to spatially control the illumination of the blue activating light (orange box, Figure 1c), and was pulsed before each image acquisition during the recruitment period. Recruitment of the prGEF to the activation region was rapid and reversible upon extinguishing the stimulating blue light (Figure 1c,d and Supplementary Movie 1).

To investigate whether recruitment of the prGEF resulted in activity of proteins downstream of RhoA, we tracked the dynamics of actin and myosin light chain (MLC) during recruitment (Figure 1e-g). Both actin and myosin accumulated in the activation regions, resulting in an increase in fluorescence intensity during the 15 min activation period (Figure 1e-g and Supplementary Movies 2-3). Interestingly, local activation of RhoA did not lead to *de novo* stress fiber assembly in the activation region (Figure 1e and Supplementary Movie 2). At the end of the activation period, fluorescence intensities of both actin and myosin returned to baseline levels. These results indicate that exogenous RhoA activation via LARG recruitment is not sufficient to maintain elevated RhoA activity and the concomitant increases in local actin and myosin concentrations. To confirm that local activation of RhoA was acting on actin and myosin through its downstream effectors, formin and ROCK, the experiments were repeated in the presence of either SMIFH2, a pan formin inhibitor[38], or Y-27632, a Rho-associated Kinase inhibitor (Figure 1h). Local recruitment of actin and MLC were significantly inhibited by the presence of SMIFH2 and Y-27632, respectively. These results illustrate that RhoA

activity and recruitment of its downstream effectors can be spatially and temporally controlled via light.

Adhesion morphology is unperturbed by local RhoA activity

Previous work has suggested that focal adhesion formation and maturation are tension dependent processes driven by increased RhoA activity at adhesion sites [27,28,39]. To test these hypotheses we examined how local RhoA activation affected traction forces and focal adhesions. Cells expressing mCherry-vinculin, a marker of focal adhesions, were plated on polyacrylamide gels coated with fibronectin and traction stresses were measured via Traction Force Microscopy (Figure 2a,b and Supplementary Movie 4)[40,41]. During local activation of RhoA, traction stresses increased at focal adhesion sites, on a similar timescale to that of myosin localization (Figure 1g). Despite the increased force, the total number of adhesions remained essentially constant (Figure 2c). Individual adhesion morphology and vinculin intensity were also unaffected, despite large increases in stress at a majority of previously established adhesion sites during local RhoA activation (Figure 2d & Supplementary Fig. S1). Too much illumination, however, results in adhesion failure and detachment from the substrate (Supplementary Fig. S2). As the adhesions and stress fibers are fully formed already in these cells, the lack of change in adhesion morphology is consistent with previous results showing that adhesion size and tension are correlated during the initial growth phase of the adhesion[42], and that adhesion maturation is driven by proximal actin stress fiber assembly[43].

To determine the effect of local RhoA activation on the overall contractility of the cell, we used traction force microscopy to measure the total strain energy, which reflects the amount of mechanical work done by the cell on its environment[44]. Activation induced a rapid increase in both traction stresses and strain energy (Figure 2b,c). At the end of the activation period, the strain energy decreased to their original baseline values (Figure 2c). Interestingly, traction stresses were mostly seen to increase at the cell periphery, where traction stresses were already established, and in areas immediately adjacent to the activation region. No change was seen in the activation area itself (Figure 2b). This suggests that locally generated forces balance within the activation region and only unbalanced forces at the edge of

this region are turned into productive traction forces. Thus, a local increase of tension leads to globally distributed traction forces at pre-existing focal adhesions.

Cells maintain a contractile set point

That cells return to a similar baseline contractility following a period of exogenous RhoA activation is consistent with previously established ideas of tensional homeostasis[44-47]. To explicitly probe this behavior, we performed a series of local activations of different sizes on a single cell (Figure 2e and Supplementary Movie 5). After measuring the strain energy at an initial steady state, a cell was exposed to three 15 min periods of local RhoA activation of increasing size with relaxation periods between each activation (Figure 2e,f). The strain energy increased concomitant with the size of the activation region. During activation, both local stresses immediately surrounding the activation region, and long-range stresses at the cell periphery could be seen to increase (Figure 2e). Following each activation, the strain energy returned to the initial baseline level (Figure 2f).

To elucidate the underlying mechanical principles, we built a physical model that would capture this physical response. We constructed a model of the cell as a continuum of contractile elements in series, each with one elastic and one viscous element in parallel (Figure 2g). Such a model is known as an "active Maxwell fluid" and is used here because we are interested in long time scales, when the system is expected to flow[21,25,48]. Contractility was assumed to increase with an exponentially plateauing ramp in the activated region, consistent with the observed accumulation profiles for actin and myosin (Figure 1g), and the substrate was represented as an elastic spring coupled to the cell by a friction element. The model parameters for the elastic modulus, viscosity, friction and contractility were found by fitting the model to the strain energy data, while the value of the substrate stiffness was fixed. This procedure resulted in a curve in good agreement with the experimental data (Figure 2f).

We find that both the viscous and elastic elements are necessary to accurately capture the behavior of the system over the whole time course of ramping, plateau and relaxation. The ratio of viscosity to elasticity defines a viscoelastic relaxation time of approximately 60 minutes; this time scale determines the transition from when the cytoskeleton behaves predominately elastic-like (< 60 min) to

144 predominately fluid-like (> 60 min). Our results thus indicate that stress fibers are predominantly
145 elastic on the scale of tens of minutes, despite proteins within the stress fiber turning over on
146 timescales of tens of seconds[15]. This strong elastic behavior is also consistent with the immediate
147 increase in cell traction stresses at the cell periphery (Figure 2b,e) upon local activation of RhoA in the
148 center of the cell.
149
150 **Stress fibers contract independent of the background network**
151 To investigate the cytoskeletal architectures that give rise to this strong contractility, we tracked
152 myosin dynamics during local RhoA activation. In the steady state, as new actomyosin is polymerized
153 and incorporated into stress fibers, there is a retrograde flow of actomoysin from the periphery
154 towards the cell center[15,17]. Using particle image velocimetry (PIV)[49,50] we measured both the local
155 direction and magnitude of myosin flow. We found that myosin flow rates along the stress fiber
156 increased as myosin accumulated in the activation region creating a local contraction, and that this
157 flow was directed along the orientation of the stress fibers spanning the activation region (Figure 3a,b,
158 Supplementary Fig. S3, and Supplementary Movie 6). The flow direction was independent of the
159 activation region geometry, with the direction always being determined by the stress fiber orientation
160 (Supplementary Movie 7).
161
162 The cytoskeleton of a strongly adherent cell is typically thought to be a 2D material comprised of stress
163 fibers embedded in an isotropic cortex[41,51,52]. Since flows induced by local RhoA activation appear to
164 track the orientation of the stress fibers (Figs. 3a,b and S2), we sought to address the relative
165 contractile contributions of the stress fibers and the actin networks. We therefore built a 2D discrete
166 model analogous to the 1D continuum model described above (Figure 3c). The model consists of a
167 triangular mesh with the contractile elements again connected in parallel to the viscous and elastic
168 elements, with lines of increased contractility representing the stress fibers. Using a simple rectangular
169 cell, we first verified that, without stress fibers, this model recapitulates the results from the one-
170 dimensional continuum model (Figure 3d). Similar to the 1D model above, the contractile components
171 in a region in the center of the cell were slowly increased with an exponentially plateauing ramp. The

parameters were then adjusted so that the model both qualitatively and quantitatively recapitulated the expected flow patterns of the 1D continuum model (Figure 3d).

To explore the relative contributions of the background mesh and the stress fibers, we considered two test cases: (1) If both the mesh and the stress fibers contained contractile elements, the stress fibers pinched inward transverse to their orientation during local activation (Figure 3e); and (2) when contractile elements were only included in the stress fibers (as depicted in Figure 3c), the cytoskeletal flow was restricted to directions along the stress fiber (Figure 3f), consistent with our experimental results (Figure 3a-b, Supplementary Fig. S3, and Supplementary Movies 6-7). Since transverse deformations were never seen in experiments, it is clear that the stress fibers must be the predominant contractile elements observable at this resolution which respond to local RhoA-induced contractions. Furthermore, this result illustrates that it is appropriate to think of a stress fiber as a one-dimensional contractile element with viscous and elastic components embedded in a passive viscoelastic network.

Stress fibers flow due to local RhoA induced strain

Having identified the stress fiber as the main contractile unit responding to exogenous RhoA activation, we next sought to address whether stress fibers undergo deformation during contraction. Since stress fibers can be considered as 1D structures, we analyzed myosin flow along the fiber using kymographs. A kymograph drawn along a single stress fiber illustrates that myosin puncta flowed from both ends towards the activation regions when RhoA was activated locally (Figure 4a-b, Supplementary Fig. S5). Similarly, a kymograph drawn by projecting the flow speed along the stress fiber from the velocity field created by our PIV analysis illustrates even more clearly how cytoskeletal flow was perturbed by local RhoA activation. Flow of myosin from both ends of the stress fiber reoriented towards the recruitment regions and increased from ~1 nm/s on average to more than 3 nm/s during activation (Figure 4c and Supplementary Fig. S5). Strikingly, the flow was also seen to reverse direction, flowing away from the recruitment region and towards the cell periphery, during the relaxation period following the local activation (Figure 4b,c). This flow reversal is reminiscent of the restoring force in elastic objects that restores its original shape after removal of external force (e.g. recoil of an elastic band after stretch). In

active systems, flow reversal could also arise from spatial variations in tension. Specifically, this would either require the myosin stress within the activation region to fall below its pre-activation level or increased myosin activity distal to the activation site. However, we do not observe such changes in actomyosin density, indicating a passive elastic-like element may be sufficient in describing this recoil.

We next developed a protocol to measure the magnitude of the stress fiber displacement during these periods of contraction and relaxation (Figure 4d). The displacement in a given fiber was determined by measuring the relative position of puncta along the fiber following 15 minutes of local RhoA activation and 15 minutes after it ceased. During contraction, puncta on either side of the activation region contracted on average ~3 μm from their original position before relaxing back to ~1 μm from their original position (Figure 4d). The relaxation response across many stress fibers from multiple cells could be further clustered into two groups, one which exhibited strong reversal (~80% of the original position) and one which exhibited little to no reversal (~25% of the original position) (Figure 4d).

To determine whether stress fibers were stretching due to the local contraction, we used cells expressing mApple-α-actinin, an actin crosslinker which localizes to well defined puncta on stress fibers (Figure 4e and Supplementary Movie 8). We created kymographs of α-actinin flow during local activation of RhoA and tracked paths of individual puncta (Figure 4f). The velocity of individual puncta was determined from the slope of the tracks in the kymograph and plotted as a function of distance from the activation zone (Figure 4g). Puncta along the stress fiber moved at similar speeds, indicating that, in general, the stress fiber was translating as a rigid rod during the local contraction (Figure 4g). Where present, changes in velocity between neighboring puncta were abrupt (blue arrow Fig 4g), suggesting points of structural failure along a fiber. These results indicate that the strain induced in the stress fiber is restricted to the local contraction in the activation region and discrete sites of extension in regions outside the activation region.

By fitting the experimental kymographs to both our 1D continuum and 2D discrete models, we show that similar flow patterns emerge naturally from the mechanics of the system (Figure 4h). The high elasticity of the stress fiber, specifically the ratio of elasticity to viscosity, is sufficient to recapitulate

the flow profiles that were seen during both RhoA activation and relaxation. Furthermore, the parameters found from the kymograph fitting process were consistent with the parameter values found when fitting the strain energy (Table 2).

Zyxin is recruited to sites of strain on stress fibers

In order to probe the underlying molecular basis of this elasticity, we sought to identify stress fiber-associated proteins that could contribute to the recoil behavior. Zyxin has been previously established as a mechanosensitive protein that dynamically localizes to sites of strain along stress fibers[53,54], in addition to focal adhesions[55]. Using cells expressing mCherry-zyxin, we monitored zyxin activity during RhoA activation (Figure 5a and Supplementary Movie 9). Zyxin recruitment was consistently observed in a small population of focal adhesions outside of the local activation region (Figure 5b). Surprisingly, we found that zyxin also accumulated along stress fibers in the region of local activation (Figure 5c,d). Given the myosin accumulation and direction of flow, this suggests that zyxin might be recruited to both sites of compression and extension. Paxillin, another mechanosensitive LIM domain protein that responds to stress [56,57], behaved similarly to zyxin (Supplementary Fig. S4).

Zyxin is required for stress fibers to behave elastically

To further explore the role of zyxin in stress fiber mechanical behavior we used mouse embryonic fibroblast cells derived from zyxin$^{-/-}$ mice[58]. Despite the loss of zyxin, these cells form actin stress fibers and focal adhesions and are highly contractile[59]. When we locally activated RhoA in the zyxin$^{-/-}$ cells, myosin accumulated in the activation region (Figure 5e and Supplementary Movie 10). This accumulation drove a contractile flow into the local activation area that was indistinguishable from wild type cells, indicating that loss of zyxin did not impede myosin activity. Upon stopping the GEF recruitment in zyxin$^{-/-}$ cells, cytoskeletal flow returned to pre-activation rates, consistent with the reduced local contraction, but did not reverse direction (Figure 5e-f,i, Supplementary Fig. S5, and Supplementary Movie 10). Expression of EGFP-zyxin in this cell line restored the flow reversal (Figure 5g-i, Supplementary Fig. S5 and Supplementary Movie 11). Together these results indicate that zyxin is required for the flow reversal occurring after local RhoA activation ends.

Using the kymographs produced in the zyin$^{-/-}$ and zyxin$^{-/-}$+EGFP-zyxin cells, we again fit the data to our mechanical model (Figure 5j-l, Supplementary Fig. S6). For the zyxin$^{-/-}$ cells, we found the viscoelastic relaxation time reduced to 1 sec, indicating that the stress fibers are predominately fluid-like at all physiological time scales. Rescue of the zyxin$^{-/-}$ cells with EGFP-zyxin resulted in parameter fits that were consistent with the NIH 3T3 fibroblast data. Zyxin is thus important for maintaining the qualitative mechanical response of stress fibers, ensuring they are predominately elastic at ~1 hr time scales.

Discussion

This study demonstrates that the mechanical behavior of adherent cells is strongly shaped by stress fibers and their ability for rapid force transmission even in the face of molecular turnover and flow. Using an optogenetic probe to locally activate RhoA via recruitment of the DH domain of LARG, a RhoA specific GEF, we find that we can stimulate a local contraction in stress fibers due to an increased accumulation of actin and myosin in the activation area (Figure 6, 1). This local contraction causes a tension gradient at the boundaries of the activation region and a flow towards it (Figure 6, 2). The flow of myosin and α-actinin increases the strain both on the interface coupling the stress fiber to the adhesion and in the activation region, leading to recruitment of the mechanosensitive protein zyxin (Figure 6, 3). When local activation of RhoA is stopped, the system relaxes to the pre-activation state, mainly driven by elastic energy accumulated in the strained regions, and results in a transient cytoskeletal flow of material away from the local activation region (Figure 6, 4).

This elastic behavior is dependent on zyxin. Previous reports have shown that zyxin localizes along the stress fiber at the interface of the adhesion[60,61]. This positioning suggests that previously reported zyxin mediated stress fiber repair mechanisms[56,59] are also occurring at the adhesion interface as actin is assembled and is incorporated into the stress fiber while under tension. The localization of zyxin to potential sites of compression, however, is novel. While it is known that the LIM domain of zyxin is sufficient for localization[62], the exact mechanism through which zyxin recognizes sites of strain remains unknown.

These data further illustrate that RhoA activity and its downstream effectors are tightly regulated by the cell. We see no evidence that RhoA activation alone leads to *de novo* stress fiber formation or adhesion maturation. Instead these processes likely result from concurrent changes in cytoskeletal architecture[43,63]. More interestingly, the data suggest cells regulate total RhoA activity to maintain a constant homeostasis[44-47]. Specifically, the relaxation kinetics of the downstream effectors match the kinetics of the optogenetic probe[35], thus indicating that there is no positive feedback loop whereby production of RhoA•GTP alone is sufficient to promote further activation of RhoA. To sustain a given contractile state, therefore, the cell must actively regulate and maintain a specific RhoA•GTP concentration.

By using an optogenetic approach to perturb the local mechanical balance within the cell, we were able to probe the material properties of the cytoskeleton in ways previously inaccessible. It is instructive to consider our results within the context of other approaches that probe stress fiber mechanics. One such method is the cyclic stretch of an elastic substrate, in which Rho-activation is involved in reorienting the cell and its stress fibers away from the direction of stretch[64]. It has been argued that the reorientation response might result from a homeostatic set point, that is either passive[65] or active[66] in nature, which is consistent with our experimental results. Another interesting comparison can be made with severing of stress fibers via laser ablation[53,67-69]. In severing experiments, the mechanical stability of the fiber is compromised while myosin activity on the remaining portion remains unchanged, thus driving a large contraction over seconds. By contrast, we probe the response to small perturbations in tension along an intact stress fiber over tens of minutes. As a result of the differences between the two setups, these experiments are probing different types of stress fiber mechanical response. In contrast to severing experiments, where sarcomeres have been reported to collapse to a minimal length following a reduction in tension[68], we do not see changes in the spacing of the sarcomeric structure of crosslinkers in the fiber during the increase in tension driven by local RhoA activation. Our experiments thus probe the homeostasis of the system, while severing probes the limits of stability. Interestingly, it has been reported previously that sarcomere size in stress fibers fluctuates on a 20 min time scale[70], which might be related to the 50 min viscoelastic time scale

316 revealed by our model results. Future insights could be derived from fluctuation analysis during
317 optogenetic activation.
318
319 Contraction is driven by the local accumulation of myosin in the region of activation, but the origin of
320 the elastic-like recovery is less clear. We see no evidence of additional myosin accumulation in distal
321 portions of the stress fiber during the relaxation, suggesting that the recoil arises from zyxin-mediated
322 repair mechanisms within stress fibers. This is further supported by the fact that the zyxin$^{-/-}$ cells
323 exhibit identical contractile behavior, but none of the elastic recoil. Zyxin is known to recruit actin
324 polymerization factors like VASP and actin crosslinkers like alpha-actinin[59] and these interactions might
325 be essential to ensure mechanical integrity of stress fibers. The molecular detail of these protein
326 interactions under applied load remains an outstanding question.
327
328 Our experiments highlight the importance of defining the relevant timescales and perturbations when
329 describing a material as elastic or viscous. Given that typical turnover rates for proteins in the
330 cytoskeleton are on the order of tens of seconds[15,25,26], it is surprising that our model results suggest
331 that stress fibers have elastic-like properties on timescales of ~1 hour. The viscous behavior of cells is
332 typically associated with irreversible changes brought on through remodeling and dynamic activity of
333 proteins (e.g. cytoskeletal remodeling during migration)[21,71]. This has informed much of the active fluid
334 theoretical frameworks that have been developed[21]. Conversely, elasticity has typically been used to
335 describe cellular material properties without consideration of the dynamic activity of the
336 components[44,72,73] and has been used in understanding force generation[44] and mechanosensing[74]. Our
337 results suggest that active remodeling within the cytoskeleton can result in elastic-like properties of
338 time scales exceeding those of dynamics of internal components. Moreover, our results indicate that
339 very different viscoelastic time scales might co-exist in the same cell and even in the same cytoskeletal
340 structures. Finally, our results implicate an important role for zyxin in regulating transitions between
341 fluid-like and elastic-like behaviors. This has exciting implications for interpreting the underlying
342 physics of active cytoskeletal materials. The fact that this behavior can be controlled by the activity of a
343 single protein suggests intriguing potential mechanisms cells can use to regulate their mechanical
344 properties during morphogenesis and development.

Methods

Cell culture and transfection

NIH 3T3 fibroblasts (American Type Culture Collection, Manassas, VA) were cultured in DMEM media (Mediatech, Herndon, VA) and supplemented with 10% FBS (HyClone; ThermoFisher Scientific, Hampton, NH), 2 mM L-glutamine (Invitrogen, Caarlsbad, CA) and penicillin-streptomycin (Invitrogen). Zyxin$^{-/-}$ and zyxin$^{-/-}$+EGFP-zyxin Mouse Embryonic Fibroblast cells were a gift of Mary Beckerle's lab (University of Utah, Salt Lake City, UT) and cultured similarly to the NIH 3T3 fibroblasts[59]. Cells were tested for mycoplasma and were free of contamination. All cells were transiently transfected via electroporation 24 hrs prior to experiment using a Neon Transfection system (ThermoFisher Scientific). Following transfection, cells were plated on glass coverslips and imaged the next day.

Drug treatments

Cells were treated with either the 10 µM SMIFH2 a pan-formin inhibitor[38] or 1µM of Y-27632 which inhibits ROCK (ThermoFisher Scientific), for at least 30 minutes prior to imaging.

Plasmids

The optogenetic membrane tether consisting of Stargazin-GFP-LOVpep and prGEF constructs used are previously described (Wagner 2016). prGEF-YFP was constructed in an identical manner to prGEF with YFP replacing mCherry. This construct was used in experiments where the effects on various downstream markers were visualized. To examine effects on the actin and myosin networks, we used mApple-Actin and mApple-MLC constructs (gifts from M Davidson, University of Florida, Gainesville FL), mCherry-Vinculin (gift from V Weaver, University of California at San Francisco, San Francisco, CA) and mCherry-zyxin (gift from M Beckerle, University of Utah, Salt Lake City, UT).

Live cell imaging

Glass coverslips were placed in a Chamlide magnetic chamber (Live Cell Instrument, Seoul, Korea) in culture media supplemented with 10 mM HEPES and 30µL/mL Oxyrase (Oxyrase Inc., Mansfield, OH) and maintained at 37˚C. Cells were imaged on an inverted Nikon Ti-E microscope (Nikon, Melville, NY) with a Yokogawa CSU-X confocal scanhead (Yokogawa Electric, Tokyo, Japan), and laser merge module

374 containing 491nm, 561nm, and 642nm laser lines (Spectral Applied Research, Ontario, Canada). Images
375 were collected on either a CoolSNAP HQ2 CCD (Roper Scientific, Trenton, NJ) or Zyla 4.2 sCMOS
376 Camera (Andor, Belfast, United Kingdom). Local recruitment using the optogenetic probe was
377 performed using a 405 nM laser coupled to a Mosaic digital micromirror device (Andor). Images were
378 collected using a 60x 1.49 NA ApoTIRF oil immersion objective (Nikon). All hardware was controlled
379 using MetaMorph Automation and Image Analysis Software (Molecular Devices, Sunnyvale, CA).
380
381 Unless otherwise stated, cells were imaged in the 561 channel every 20 s for 45 min, with the first 15
382 min used to determine the steady state of the system, the second 15 min to perform local recruitment,
383 and the final 15 min to record any recovery. During recruitment a local region drawn in MetaMorph
384 was illuminated by the 405nm laser for 960 ms at a power < 1 μJ/s immediately prior to the acquisition
385 of each 561 image.
386
387 **Local recruitment analysis**
388 All data analysis was performed using MATLAB (Mathworks, Natick, MA). Regions of interest (ROIs)
389 were drawn to calculate the average intensity in the local recruitment region, a control area within the
390 cell but far away from the recruitment area, and a background area outside of the cell. The average
391 background intensity was subtracted from the control region and this curve was used to determine a
392 photobleaching correction. The photobleaching correction was then applied to the background
393 subtracted average intensity in the local recruitment region and normalized to the average value of the
394 first 15 min of the data.
395
396 **Focal adhesion analysis**
397 Images were thresholded and segmented to create binary masks using MATLAB. Adhesion masks were
398 filtered to exclude adhesions smaller than 0.4 μm^2 due to the inability to segment them consistently.
399 The binary mask was then used to calculate the total number and average fluorescence intensity of
400 adhesions in each frame. These masks were also used to calculate the average stress under the
401 adhesions. To calculate the percentage of adhesions which increased in intensity or stress during
402 activation, we compared the maximum intensity of the adhesion during activation to the intensity

403 immediately prior to activation. Adhesions were considered to have shown an increase in either
404 intensity or stress if the magnitude of the increase was greater than 10%.
405
406 **Kymograph and local displacement analysis**
407 Kymographs were created in MATLAB by drawing lines along stress fibers and averaging across a width
408 of 9 pixels. Local displacement was determined by locating a feature 5μm from the edge of the
409 activation zone in a kymograph immediately prior to activation. The location of this feature was then
410 tracked and recorded following the 15 minute period of activation, and then again following 15
411 minutes of relaxation.
412
413 **Cytoskeletal flow analysis**
414 Images were first corrected for bleaching and then filtered with a 3D Gaussian filter to remove noise.
415 Flow fields were calculated using an implementation of the Brox et al. optical flow algorithm[49,50] that
416 ensures spatial and temporal smoothness. Flow field kymographs were generated by projecting the
417 flow vectors onto the line defining the kymograph. To compare the direction of flow with the
418 organization of the cytoskeleton, the local orientation of actin fibers was extracted from the structure
419 tensor[75].
420
421 **α-actinin spacing analysis**
422 Kymographs were drawn as above. For each timepoint in the kymograph, local peaks in the linescan
423 were determined. Peaks were then connected to create tracks across the kymograph. Local velocity
424 was determined by isolating the section of the track during the activation period and fitting the
425 trajectory to a straight line. The fitted slope was taken as the velocity.
426
427 **Traction force microscopy**
428 Traction force microscopy was performed as described previously[40,41,44]. Briefly, polyacrylamide gels
429 embedded with 40-nm fluorescent microspheres (Invitrogen) were polymerized on activated glass
430 coverslips. The shear modulus of the gels used in these experiments was 8.6 kPa. Following
431 polymerization gels were washed with PBS and crosslinked with the extracellular matrix protein

fibronectin (Millipore, Billerica, MA) using the photoactivatable crosslinker sulfo-sanpah (Thermo Fisher Scientific). Cells were plated and allowed to spread for at least 4 hours prior to imaging as described above.

Following imaging, cells were removed from the substrate using 0.5% sodium dodecyl sulfate and a reference image of the fluorescent beads in the unstrained substrate was taken. The image stack was then aligned to correct for drift and compared to the reference image using particle imaging velocimetry to create a displacement field with a grid spacing of 0.86 μm. Displacement vectors were filtered and interpolated using the Kriging interpolation method. Traction stresses were reconstructed via Fourier Transform Traction Cytometry[40,76], with a regularization parameter chosen by minimizing the L2 curve[41]. The strain energy was calculated as one half the integral of the traction stress field dotted into the displacement field[44].

Statistical analysis

All experiments were repeated a minimum of 3 times. Cells presented in figures are representative samples of the population behavior. Box plots represent the 25th, 50th and 75th percentiles of the data. Whiskers on the boxplot extend to the most extreme data points not considered outliers. Error bars represent the standard deviation, except where noted otherwise. Statistical significance was determined using independent two-sample Student's *t* tests of the mean to compare groups of data. Statistical significance is indicated by asterisks: (*) represents a p-value < 0.05; (**) represents a p-value < 0.01.

Code availability

Matlab analysis routines can be made available upon request to the corresponding author.

Data availability

The data that support the findings of this study are available from the corresponding author upon reasonable request. Stargazin-GFP-LOVpep and prGEF plasmids are available on addgene.

References:

1. Lecuit, T., Lenne, P.-F. & Munro, E. Force generation, transmission, and integration during cell and tissue morphogenesis. *Annu Rev Cell Dev Biol* **27,** 157–184 (2011).
2. Paluch, E. & Heisenberg, C.-P. Biology and Physics of Cell Shape Changes in Development. *Current Biology* **19,** R790–R799 (2009).
3. Iskratsch, T., Wolfenson, H. & Sheetz, M. P. Appreciating force and shape—the rise of mechanotransduction in cell biology. *Nat Rev Mol Cell Biol* **15,** 825–833 (2014).
4. Murrell, M., Oakes, P. W., Lenz, M. & Gardel, M. L. Forcing cells into shape: the mechanics of actomyosin contractility. *Nat Rev Mol Cell Biol* **16,** 486–498 (2015).
5. Martin, A. C., Gelbart, M., Fernandez-Gonzalez, R., Kaschube, M. & Wieschaus, E. F. Integration of contractile forces during tissue invagination. *J Cell Biol* **188,** 735–749 (2010).
6. Wagner, E. & Glotzer, M. Local RhoA activation induces cytokinetic furrows independent of spindle position and cell cycle stage. *J Cell Biol* **213,** 641–649 (2016).
7. Melvin, A. T., Welf, E. S., Wang, Y., Irvine, D. J. & Haugh, J. M. In chemotaxing fibroblasts, both high-fidelity and weakly biased cell movements track the localization of PI3K signaling. *Biophys J* **100,** 1893–1901 (2011).
8. Plotnikov, S. V. & Waterman, C. M. Guiding cell migration by tugging. *Curr Opin Cell Biol* **25,** 619–626 (2013).
9. McBeath, R., Pirone, D. M., Nelson, C. M., Bhadriraju, K. & Chen, C. S. Cell shape, cytoskeletal tension, and RhoA regulate stem cell lineage commitment. *Dev Cell* **6,** 483–495 (2004).
10. Wang, A. *et al.* Nonmuscle myosin II isoform and domain specificity during early mouse development. *Proc. Natl. Acad. Sci. U.S.A.* **107,** 14645–14650 (2010).
11. Müller, T. *et al.* Non-muscle myosin IIA is required for the development of the zebrafish glomerulus. *Kidney Int.* **80,** 1055–1063 (2011).
12. Schwarz, U. S. & Gardel, M. L. United we stand - integrating the actin cytoskeleton and cell-matrix adhesions in cellular mechanotransduction. *J Cell Sci* **125,** 3051–3060 (2012).
13. Blanchoin, L., Boujemaa-Paterski, R., Sykes, C. & Plastino, J. Actin dynamics, architecture, and mechanics in cell motility. *Physiol Rev* **94,** 235–263 (2014).
14. Fletcher, D. A. & Mullins, R. D. Cell mechanics and the cytoskeleton. *Nature* **463,** 485–492 (2010).
15. Hotulainen, P. & Lappalainen, P. Stress fibers are generated by two distinct actin assembly mechanisms in motile cells. *J Cell Biol* **173,** 383–394 (2006).
16. Devreotes, P. & Horwitz, A. R. Signaling Networks that Regulate Cell Migration. *Cold Spring Harb Perspect Biol* **7,** a005959 (2015).
17. Gardel, M. L., Schneider, I. C., Aratyn-Schaus, Y. & Waterman, C. M. Mechanical integration of actin and adhesion dynamics in cell migration. *Annu Rev Cell Dev Biol* **26,** 315–333 (2010).
18. Hoffman, B. D. & Crocker, J. C. Cell mechanics: dissecting the physical responses of cells to force. *Annu Rev Biomed Eng* **11,** 259–288 (2009).
19. Stricker, J., Falzone, T. & Gardel, M. L. Mechanics of the F-actin cytoskeleton. *J Biomech* **43,** 9–14 (2010).
20. Zhu, C., Bao, G. & Wang, N. Cell mechanics: mechanical response, cell adhesion, and molecular deformation. *Annu Rev Biomed Eng* **2,** 189–226 (2000).
21. Prost, J., Julicher, F. & Joanny, J.-F. Active gel physics. *Nature Physics* **11,** 111–117 (2015).

22. Schwarz, U. S. & Safran, S. A. Physics of adherent cells. *Rev Mod Phys* **85,** 1327 (2013).
23. Broedersz, C. P. & Mackintosh, F. C. Modeling semiflexible polymer networks. *Rev Mod Phys* **86,** 995 (2014).
24. Fritzsche, M., Lewalle, A., Duke, T., Kruse, K. & Charras, G. Analysis of turnover dynamics of the submembranous actin cortex. *Mol Biol Cell* **24,** 757–767 (2013).
25. Saha, A. *et al.* Determining Physical Properties of the Cell Cortex. *Biophys J* **110,** 1421–1429 (2016).
26. Hu, S. *et al.* Long-range self-organization of cytoskeletal myosin II filament stacks. *Nat Cell Biol* (2017). doi:10.1038/ncb3466
27. Ridley, A. J. & Hall, A. The small GTP-binding protein rho regulates the assembly of focal adhesions and actin stress fibers in response to growth factors. *Cell* **70,** 389–399 (1992).
28. Chrzanowska-Wodnicka, M. & Burridge, K. Rho-stimulated contractility drives the formation of stress fibers and focal adhesions. *J Cell Biol* **133,** 1403–1415 (1996).
29. Machacek, M. *et al.* Coordination of Rho GTPase activities during cell protrusion. *Nature* **461,** 99–103 (2009).
30. Pertz, O., Hodgson, L., Klemke, R. L. & Hahn, K. M. Spatiotemporal dynamics of RhoA activity in migrating cells. *Nature* **440,** 1069–1072 (2006).
31. Wu, Y. I. *et al.* A genetically encoded photoactivatable Rac controls the motility of living cells. *Nature* **461,** 104–108 (2009).
32. Weitzman, M. & Hahn, K. M. Optogenetic approaches to cell migration and beyond. *Curr Opin Cell Biol* **30,** 112–120 (2014).
33. Wu, J. *et al.* Actomyosin pulls to advance the nucleus in a migrating tissue cell. *Biophys J* **106,** 7–15 (2014).
34. Valon, L., Marín-Llauradó, A., Wyatt, T., Charras, G. & Trepat, X. Optogenetic control of cellular forces and mechanotransduction. *Nat Commun* **8,** 14396 (2017).
35. Strickland, D. *et al.* TULIPs: tunable, light-controlled interacting protein tags for cell biology. *Nat Methods* **9,** 379–384 (2012).
36. Guilluy, C. *et al.* The Rho GEFs LARG and GEF-H1 regulate the mechanical response to force on integrins. *Nat Cell Biol* **13,** 722–727 (2011).
37. Jaiswal, M. *et al.* Mechanistic insights into specificity, activity, and regulatory elements of the regulator of G-protein signaling (RGS)-containing Rho-specific guanine nucleotide exchange factors (GEFs) p115, PDZ-RhoGEF (PRG), and leukemia-associated RhoGEF (LARG). *J Biol Chem* **286,** 18202–18212 (2011).
38. Rizvi, S. A. *et al.* Identification and characterization of a small molecule inhibitor of formin-mediated actin assembly. *Chem Biol* **16,** 1158–1168 (2009).
39. Balaban, N. Q. *et al.* Force and focal adhesion assembly: a close relationship studied using elastic micropatterned substrates. *Nat Cell Biol* **3,** 466–472 (2001).
40. Sabass, B., Gardel, M., Waterman, C. M. & Schwarz, U. S. High resolution traction force microscopy based on experimental and computational advances. *Biophys J* **94,** 207–220 (2008).
41. Soiné, J. R. D. *et al.* Model-based Traction Force Microscopy Reveals Differential Tension in Cellular Actin Bundles. *PLoS Comput Biol* **11,** e1004076 (2015).
42. Stricker, J., Aratyn-Schaus, Y., Oakes, P. W. & Gardel, M. L. Spatiotemporal constraints on the force-dependent growth of focal adhesions. *Biophys J* **100,** 2883–2893 (2011).
43. Oakes, P. W., Beckham, Y., Stricker, J. & Gardel, M. L. Tension is required but not sufficient for

548 focal adhesion maturation without a stress fiber template. *J Cell Biol* **196,** 363–374 (2012).
549 44. Oakes, P. W., Banerjee, S., Marchetti, M. C. & Gardel, M. L. Geometry regulates traction stresses
550 in adherent cells. *Biophys J* **107,** 825–833 (2014).
551 45. Brown, R. A., Prajapati, R., McGrouther, D. A., Yannas, I. V. & Eastwood, M. Tensional
552 homeostasis in dermal fibroblasts: mechanical responses to mechanical loading in three-
553 dimensional substrates. *J Cell Physiol* **175,** 323–332 (1998).
554 46. Ingber, D. E. Tensegrity I. Cell structure and hierarchical systems biology. *J Cell Sci* **116,** 1157–
555 1173 (2003).
556 47. Webster, K. D., Ng, W. P. & Fletcher, D. A. Tensional Homeostasis in Single Fibroblasts. *Biophys J*
557 **107,** 146–155 (2014).
558 48. Turlier, H., Audoly, B., Prost, J. & Joanny, J.-F. Furrow constriction in animal cell cytokinesis.
559 *Biophys J* **106,** 114–123 (2014).
560 49. Brox, T., Bruhn, A., Papenberg, N. & Weickert, J. in *Computer Vision - ECCV 2004* 25–36 (Springer
561 Berlin Heidelberg, 2004). doi:10.1007/978-3-540-24673-2_3
562 50. Sánchez, J., Monzón, N. & Salgado, A. Robust Optical Flow Estimation. *Image Processing On Line*
563 **3,** 252–270 (2013).
564 51. Cai, Y. *et al.* Cytoskeletal coherence requires myosin-IIA contractility. *J Cell Sci* **123,** 413–423
565 (2010).
566 52. Xu, K., Babcock, H. P. & Zhuang, X. Dual-objective STORM reveals three-dimensional filament
567 organization in the actin cytoskeleton. *Nat Methods* **9,** 185–188 (2012).
568 53. Colombelli, J. *et al.* Mechanosensing in actin stress fibers revealed by a close correlation
569 between force and protein localization. *J Cell Sci* **122,** 1665–1679 (2009).
570 54. Yoshigi, M., Hoffman, L. M., Jensen, C. C., Yost, H. J. & Beckerle, M. C. Mechanical force mobilizes
571 zyxin from focal adhesions to actin filaments and regulates cytoskeletal reinforcement. *J Cell Biol*
572 **171,** 209–215 (2005).
573 55. Zaidel-Bar, R., Ballestrem, C., Kam, Z. & Geiger, B. Early molecular events in the assembly of
574 matrix adhesions at the leading edge of migrating cells. *J Cell Sci* **116,** 4605–4613 (2003).
575 56. Smith, M. A. *et al.* LIM domains target actin regulators paxillin and zyxin to sites of stress fiber
576 strain. *PLoS ONE* **8,** e69378 (2013).
577 57. Smith, M. A., Hoffman, L. M. & Beckerle, M. C. LIM proteins in actin cytoskeleton
578 mechanoresponse. *Trends Cell Biol* **24,** 575–583 (2014).
579 58. Hoffman, L. M. *et al.* Genetic ablation of zyxin causes Mena/VASP mislocalization, increased
580 motility, and deficits in actin remodeling. *J Cell Biol* **172,** 771–782 (2006).
581 59. Smith, M. A. *et al.* A zyxin-mediated mechanism for actin stress fiber maintenance and repair.
582 *Dev Cell* **19,** 365–376 (2010).
583 60. Guo, W.-H. & Wang, Y.-L. Retrograde fluxes of focal adhesion proteins in response to cell
584 migration and mechanical signals. *Mol Biol Cell* **18,** 4519–4527 (2007).
585 61. Kanchanawong, P. *et al.* Nanoscale architecture of integrin-based cell adhesions. *Nature* **468,**
586 580–584 (2010).
587 62. Uemura, A., Nguyen, T.-N., Steele, A. N. & Yamada, S. The LIM domain of zyxin is sufficient for
588 force-induced accumulation of zyxin during cell migration. *Biophys J* **101,** 1069–1075 (2011).
589 63. Aratyn-Schaus, Y., Oakes, P. W. & Gardel, M. L. Dynamic and structural signatures of lamellar
590 actomyosin force generation. *Mol Biol Cell* **22,** 1330–1339 (2011).
591 64. Jungbauer, S., Gao, H., Spatz, J. P. & Kemkemer, R. Two characteristic regimes in frequency-

dependent dynamic reorientation of fibroblasts on cyclically stretched substrates. *Biophys J* **95,** 3470–3478 (2008).

65. Livne, A., Bouchbinder, E. & Geiger, B. Cell reorientation under cyclic stretching. *Nat Commun* **5,** 3938 (2014).
66. De, R., Zemel, A. & Safran, S. A. Dynamics of cell orientation. *Nat Phys* **3,** 655–659 (2007).
67. Kumar, S. *et al.* Viscoelastic retraction of single living stress fibers and its impact on cell shape, cytoskeletal organization, and extracellular matrix mechanics. *Biophys J* **90,** 3762–3773 (2006).
68. Russell, R. J., Xia, S.-L., Dickinson, R. B. & Lele, T. P. Sarcomere mechanics in capillary endothelial cells. *Biophys J* **97,** 1578–1585 (2009).
69. Kassianidou, E., Brand, C. A., Schwarz, U. S. & Kumar, S. Geometry and network connectivity govern the mechanics of stress fibers. *Proc. Natl. Acad. Sci. U.S.A.* **114,** 2622–2627 (2017).
70. Russell, R. J. *et al.* Sarcomere length fluctuations and flow in capillary endothelial cells. *Cytoskeleton (Hoboken)* **68,** 150–156 (2011).
71. Callan-Jones, A. C. & Voituriez, R. Active gel model of amoeboid cell motility. *New J Phys* **15,** 025022 (2013).
72. Edwards, C. M. & Schwarz, U. S. Force localization in contracting cell layers. *Phys Rev Lett* **107,** 128101 (2011).
73. Farsad, M. & Vernerey, F. J. An XFEM-based numerical strategy to model mechanical interactions between biological cells and a deformable substrate. *Int J Numer Meth Engng* **92,** 238–267 (2012).
74. Bischofs, I. & Schwarz, U. Cell organization in soft media due to active mechanosensing. **100,** 9274–9279 (2003).
75. Weichsel, J., Urban, E., Small, J. V. & Schwarz, U. S. Reconstructing the orientation distribution of actin filaments in the lamellipodium of migrating keratocytes from electron microscopy tomography data. *Cytometry A* **81,** 496–507 (2012).
76. Butler, J. P., Tolić-Nørrelykke, I. M., Fabry, B. & Fredberg, J. J. Traction fields, moments, and strain energy that cells exert on their surroundings. *Am J Physiol Cell Physiol* **282,** C595–605 (2002).

Acknowledgements

E.K.W. was supported by NIGMS T32 GM007183. C.A.B. and U.S.S. acknowledge support by the Heidelberg Karlsruhe Research Partnership (HEIKA). U.S.S. is a member of the cluster of excellence CellNetworks and the Interdisciplinary Center for Scientific Computing at Heidelberg. This work was also supported by NIGMS GM085087 to M.G. and NIH R01-GM104032 to M.L.G.

Author Contributions

P.W.O, E.K.W, M.G. and M.L.G conceived the study and designed the experiments. P.W.O and E.K.W. performed experiments. P.W.O. and M.L. performed data analysis. E.K.W. designed and cloned the molecular constructs. C.A.B., D.P., M.L. and U.S.S. conceived and designed the theoretical model. C.A.B. and D.P. performed simulations. P.W.O., M.G. U.S.S. and M.L.G. wrote the manuscript with feedback from all authors.

Competing Interests

The authors declare no competing financial interests.

638 **Figure Captions**

639 **Figure 1**

640 RhoA activity can be spatiotemporally controlled via an optogenetic probe. (**a**) Spatiotemporal control
641 of RhoA activity is achieved using an optogenetic probe to recruit the RhoA specific GEF LARG to the
642 plasma membrane. A LOVpep molecule is anchored to the membrane via fusion to the transmembrane
643 protein Stargazin, while a protein consisting of tandem PDZ domains fused to the DH domain of LARG
644 (prGEF) is distributed throughout the cytosol. Upon stimulation with 405nm light, the LOVpep
645 undergoes a conformational change exposing a high-affinity binding site which drives the prGEF to the
646 membrane where it can activate RhoA. When the activating light is removed, the LOVpep undergoes a
647 thermodynamically driven refolding halting further recruitment of prGEF. (**b**) The RhoA signaling
648 pathway. RhoA*GTP activates both Dia and ROCK, which in turn promote actin polymerization and
649 myosin II activation, respectively. (**c**) Representative images of a 3T3 fibroblast expressing an mCherry-
650 tagged version of prGEF. Upon local activation (top row – orange box) mCherry-prGEF rapidly
651 accumulates in the activation region. Removal of the activating light (bottom row) results in the
652 accumulated mCherry-prGEF dispersing back into the cytosol. (**d**) Quantification of the local intensity
653 increase of mCherry-prGEF in the activation region of the cell shown in **c**. The activation period is
654 indicated by a blue background. (**e-f**) Representative images of cells expressing either mApple-Actin (**e**)
655 or mApple-Myosin Light Chain (**f**) prior to activation, following 15 minutes of activation in the region
656 indicated, and following 15 minutes of relaxation. Both actin and myosin exhibit increases in intensity
657 in the local region of activation. (**g**) Quantification of the local intensity increase of actin and myosin
658 from the cells in **e-f**. Both signals begin increasing immediately upon RhoA activation, and dissipate as
659 soon as the activating light is switched off. (**h**) Mean maximum intensity fold-increase of actin (n=6) or
660 myosin (n=11) in regions of activation in control cells, or cells treated with 10 µM SMIFH2 (Dia
661 inhibitor; n = 7) or 1µM Y-27632 (ROCK inhibitor; n=6). Inhibition of either Dia or ROCK results in
662 reduced average increases in local intensity during RhoA activation. Time is min:sec.
663
664
665
666 **Figure 2**

667

668 Increased RhoA activity leads to increased cell contractility. (**a**) A cell expressing mCherry-Vinculin is
669 shown prior to activation, after 15 minutes of activation, and after 15 minutes of relaxation. The
670 activation region is indicated by the orange box. (**b**) The corresponding traction stress maps for the
671 time series shown in **a**. (**c**) A plot showing the strain energy versus time and the number of focal
672 adhesions versus time, with the activation period indicated by the blue background. The strain energy
673 begins to increase immediately upon activation, and begins to relax as soon as the activating light is
674 removed. In contrast, the number of focal adhesions remains relatively constant and does not respond
675 to the local increase in RhoA activity. (**d**) The average stress and fluorescence intensity of a
676 representative adhesion marked by the white box in **a**. Kymographs were generated by drawing a line
677 along the long axis of the adhesion. The activation period is indicated by the orange bar above the
678 kymograph. (**e**) A sequence of traction maps from a cell exposed to a series of activations in regions of
679 different size. Time is hr:min:sec. (**f**) A plot of the experimental (black line) and theoretical (red line)
680 strain energy vs time for the cell shown in **e**. The contractile response of the cell is proportional to the
681 size of the activation region and retreats to a baseline value following each activation period. (**g**) A
682 cartoon of the continuum model used to describe the cell in **e**. The model consists of a contractile
683 element (σ_m) in parallel to a viscous (η) and an elastic element (k), connected via a frictional elements
684 (γ) to an elastic substrate (k_M).

685

686 **Figure 3**

687 Stress fibers direct contractile flow. (**a**) Fluorescence time series of a cell expressing mApple-MLC
688 shown prior and after two separate periods of activation (orange boxes). (**b**) Flow fields of myosin
689 calculated from the images in **a**. Flow is always directed along the direction of the stress fibers. (**c**) A
690 two dimensional model of the cell was created using a triangular mesh of viscoelastic-cables (k, η)
691 connected at vertices viscously coupled (γ) to the environment. Stress fibers (blue line) consisting of
692 contractile (σ_m), viscous (η_{SF}) and elastic elements (k_{SF}) were embedded in the network. Using a
693 simplified rectangular cell with this network, local RhoA activation could be simulated by activating
694 force dipoles in network links in a region in the center of the cell. (**d**) To calibrate the 2D discrete
695 model, the average flow (white box in **c**), was measured and compared to the 1D continuum model

696 presented above. (**e-f**) The 2D discrete model was used to explore two contractile scenarios: (**e**)
697 contractile stress fibers (blue) embedded in a contractile mesh (grey); and (**f**) contractile stress fibers
698 embedded in a non-contractile background. If both the stress fibers and mesh are contractile, a
699 transverse contraction pinches together the stress fibers. If only the stress fibers contract, the flow
700 profile is restricted to the orientation of the fibers, mimicking the experimental results.
701
702 **Figure 4**
703 Stress fibers behave elastically. (**a**) Image showing a cell labeled with mApple-MLC. The activation
704 regions are indicated by the orange boxes. (**b**) A kymograph drawn along the stress fiber (green line in
705 **a**). During activation periods myosin flows towards the activation regions. (**c**) A kymograph created
706 from the same region as **b** using the flow maps determined previously. Flow was projected onto the
707 stress fiber and color coded to indicate speed and direction. This flow map illustrates that during
708 relaxation periods, myosin flow reverses direction away from the activation periods. (**d**) A
709 quantification of displacement of stress fibers during contraction and relaxation. Puncta ~5 μm from
710 the activation zone were tracked and measured following 15 minutes of activation, and again following
711 15 min of relaxation (n=41 from 4 cells). Puncta translated about 3 μm from their original position, and
712 relaxed to ~1 μm from their original position elastically. The relaxation response could be further
713 broken into two groups, one with a strong reversal (~80% of their original position) and one with a
714 weak reversal (~25% of their original position). (**e**) A cell transfected with mApple-α-actinin. The
715 activation area is indicated by the orange box. (**f**) A kymograph drawn along the direction indicated in
716 **e**, overlain with tracks of the individual α-actinin puncta during activation. (**g**) The velocity of individual
717 puncta along the stress fiber is measured from the slope of the tracks and plotted against the distance
718 from the activation region. Adjacent puncta all move at approximately the same speed. Sudden
719 changes in velocity (blue arrowhead) correlate with what appear to be site of mechanical failure along
720 the stress fiber and the appearance of new puncta. The black line represents the stress fiber from **f**,
721 while the grey lines are other stress fibers from the same cell. (**h**) A representative kymograph is fit to
722 both the 1D continuum and 2D discrete models. Both models are able to recapitulate the flow patterns
723 seen experimentally.
724

Figure 5

Zyxin accumulates at sites of strain on stress fibers during local RhoA activation. (**a**) A NIH 3T3 expressing mCherry-zyxin. The activation region is indicated by the orange box. (**b**) A kymograph of a representative adhesion marked by the white box in **a**. (**c**) The average intensity of zyxin in the activation region. (**d**) A kymograph illustrating the local zyxin accumulation during activation along the green line shown in **a**. (**e**) A zyxin$^{(-/-)}$ MEF expressing mApple-MLC before activation, at peak activation, and following relaxation. Myosin accumulates as in 3T3s. (**f**) A kymograph of myosin intensity and flow speed drawn along the green line indicated in **e**. Zyxin$^{(-/-)}$ MEFS exhibit little to no elastic flow reversal. (**g**) A zyxin$^{(-/-)}$ MEF rescued with EGFP-zyxin and expressing mApple-MLC, during an activation sequence. (**h**) A kymograph of myosin and flow illustrating a strong elastic flow reversal along the line drawn in **g.** (**i**) Displacement analysis of the zyxin$^{(-/-)}$ (n=40 from 3 cells) and zyxin$^{(-/-)}$+EGFP-zyxin MEFs (n=18 from 3 cells). Without zyxin, cells do not exhibit an elastic response. (**j**) A kymograph representing the average fit of the continuum model to the zyxin$^{(-/-)}$ data. (**k**) A kymograph representing the average fit of the continuum model to the zyxin$^{(-/-)}$+EGFP-zyxin data. (**l**) The elastic (E) and viscous (η) parameters found from fitting the experimental kymographs to the continuum model (n=5 from 3 cells for condition). Without zyxin, the elasticity increases and the viscosity decreases.

Figure 6

Molecular and mechanical models of local RhoA activation in stress fibers. Molecular model: (1) Local recruitment of prGEF leads to activation of RhoA and accumulation of actin and myosin. The local increase in actin and myosin in turn stimulates a local contraction in the stress fiber. (2) The increased local contractility induces a flow of myosin and α-actinin along the stress fiber towards the activation region. (3) Increased flow induces higher strain at both the interface coupling the stress fiber to the focal adhesion and the activation region, resulting in recruitment of the mechanosensitive protein zyxin. (4) When local activation of RhoA stops, the flow reverses direction as the stress fiber relaxes elastically. Mechanical model: The stress fiber is represented as a contractile element in parallel to viscous and elastic elements. Upon local activation of RhoA, the contractile element inside the activation region is compressed, leading to extension of both the viscous and elastic elements outside

753 the region. As local activation stops, the energy stored in the elastic element allows it to relax back to
754 its original state, while the energy in the viscous element is lost.
755
756

Supplementary Movie Captions

Supplementary Movie 1

A NIH 3T3 fibroblast expressing mCherry-prGEF during a local activation of RhoA (from Figure 1c). Local activation area is indicated by the white box. Time is in min:sec.

Supplementary Movie 2

A NIH 3T3 fibroblast expressing mApple-Actin during local activation of RhoA (from Figure 1e). Local activation area is indicated by the white box. Time is in min:sec.

Supplementary Movie 3

A NIH 3T3 fibroblast expressing mApple-MLC during a local activation of RhoA (from Figure 1f). Local activation area is indicated by the white box. Time is in min:sec.

Supplementary Movie 4

A NIH 3T3 fibroblast expressing mCherry-vinculin during a local activation of RhoA (from Figure 2a) and the corresponding traction stress maps (from Figure 2b). Local activation is indicated by the white box. Time is in min:sec.

Supplementary Movie 5

Traction stress maps of a NIH 3T3 fibroblast during a series of local RhoA activations (from Figure 2e). Local activation is indicated by white boxes. Time is in hr:min:sec.

Supplementary Movie 6

A NIH 3T3 fibroblast expressing mApple-MLC during a local activation of RhoA and the corresponding cytoskeletal flow maps (from Figure 3a,b). Local activation is indicated by white boxes. Time is in hr:min:sec.

Supplementary Movie 7

A NIH 3T3 fibroblast expressing mApple-MLC during 3 sequential local activations of RhoA. Each activation is the same area but of a different geometry. Local activation is indicated by white boxes. Time is in hr:min:sec.

Supplementary Movie 8

A NIH 3T3 fibroblast expressing mApple-α-actinin during a local activation of RhoA (from Figure 4e). Local activation is indicated by white boxes. Time is in min:sec.

Supplementary Movie 9

A NIH 3T3 fibroblast expressing mCherry-Zyxin during a local activation of RhoA (from Figure 5a). Local activation is indicated by white boxes. Time is in min:sec.

Supplementary Movie 10

A zyxin$^{(-/-)}$ Mouse Embryonic Fibroblast expressing mApple-MLC during a local activation of RhoA (from Figure 5e). Local activation is indicated by white boxes. Time is in min:sec.

Supplementary Movie 11

A zyxin$^{(-/-)}$+EGFP-zyxin Mouse Embryonic Fibroblast expressing mApple-MLC during a local activation of RhoA (from Figure 5g). Local activation is indicated by white boxes. Time is in min:sec.

807 **Figure 1**

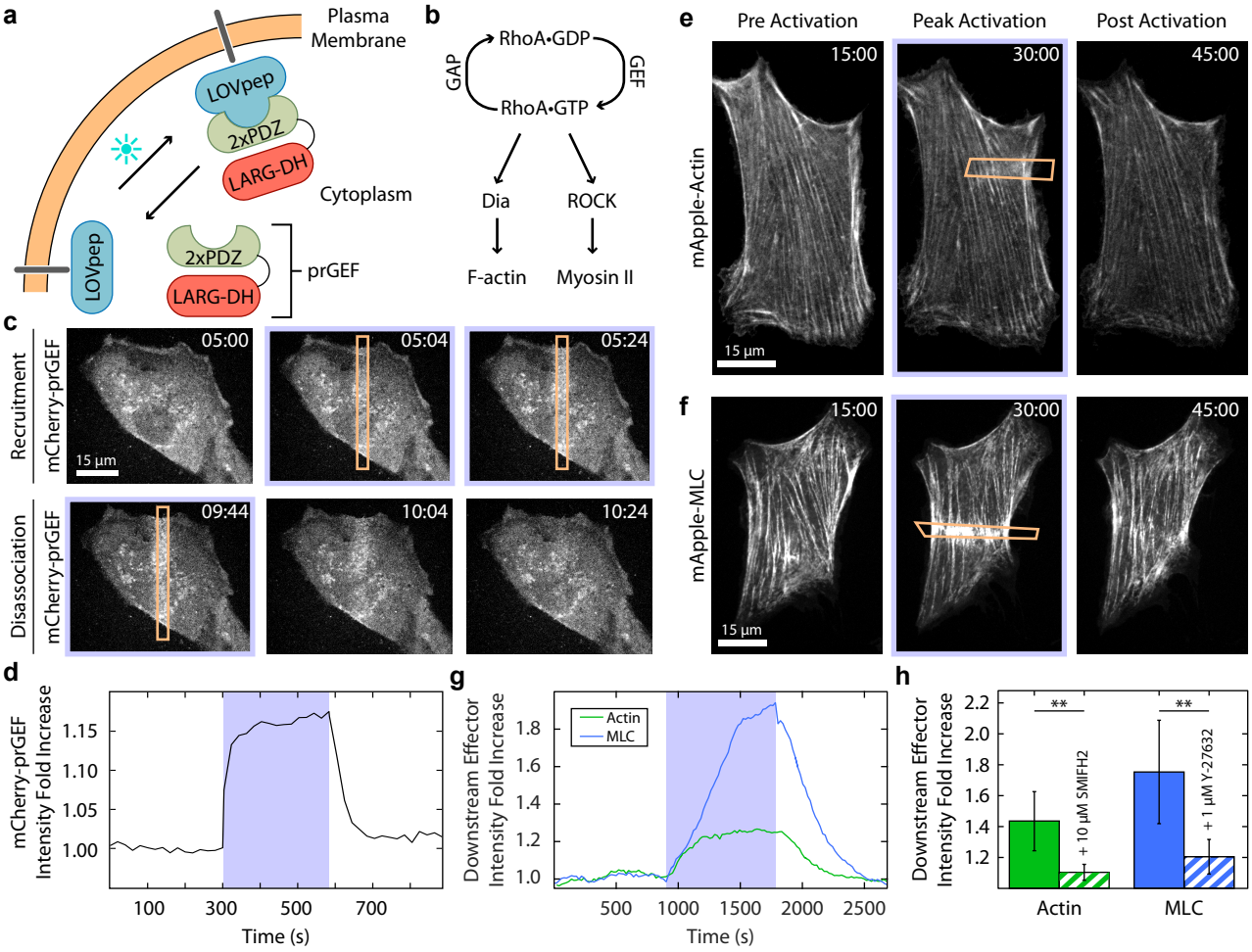

808

809

Figure 2

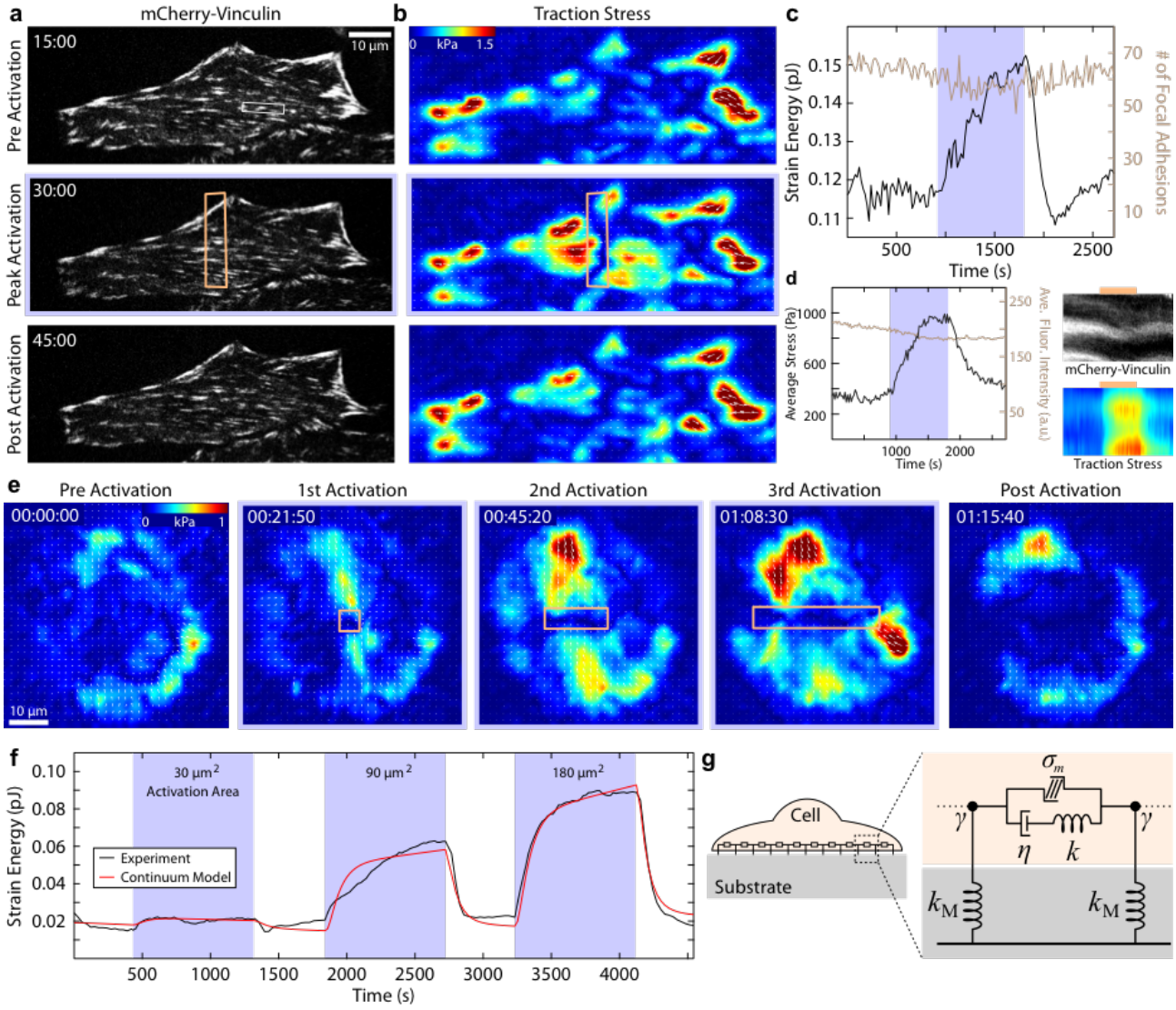

Figure 3

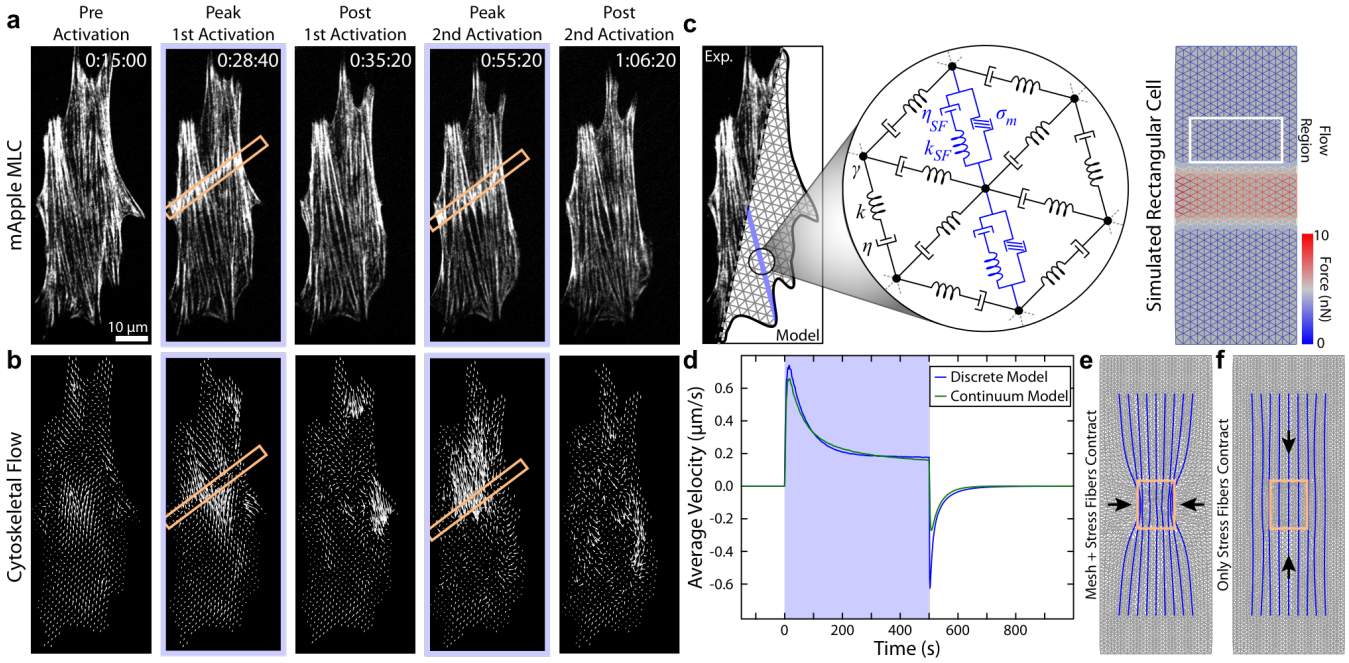

816 **Figure 4**

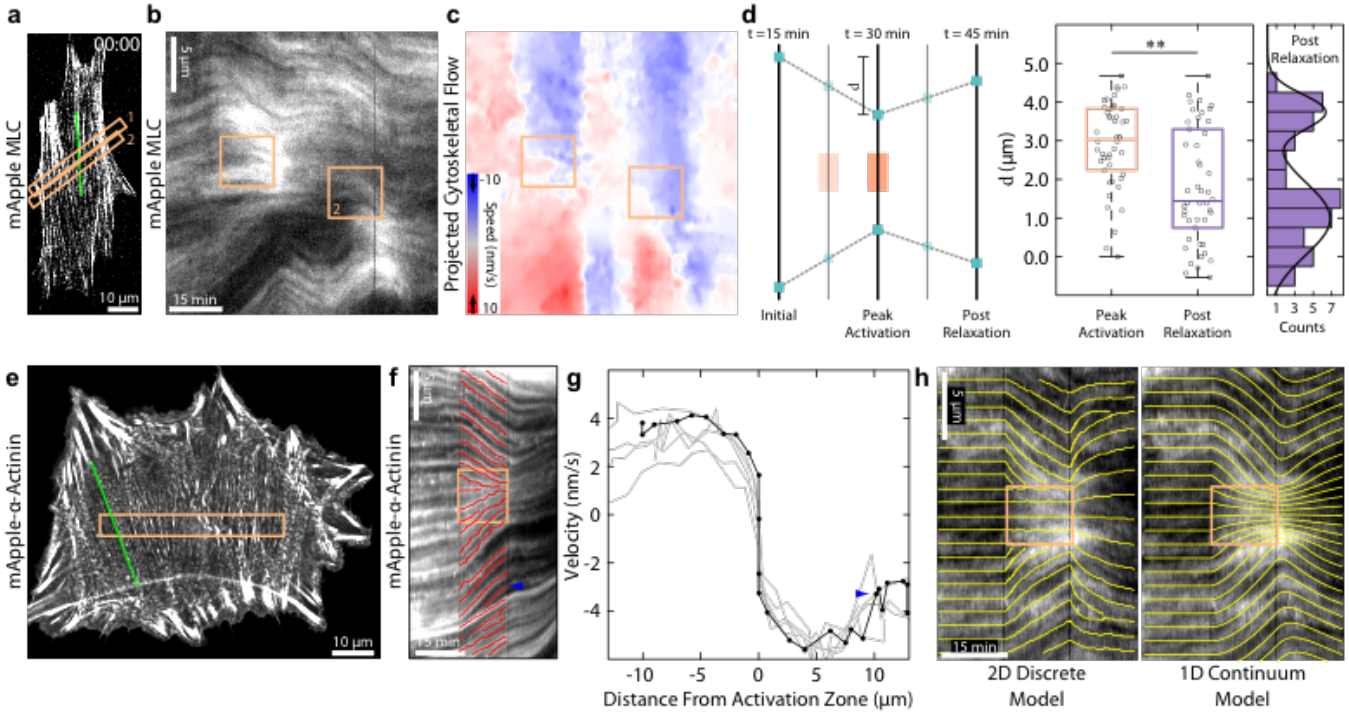

817

818

819 **Figure 5**

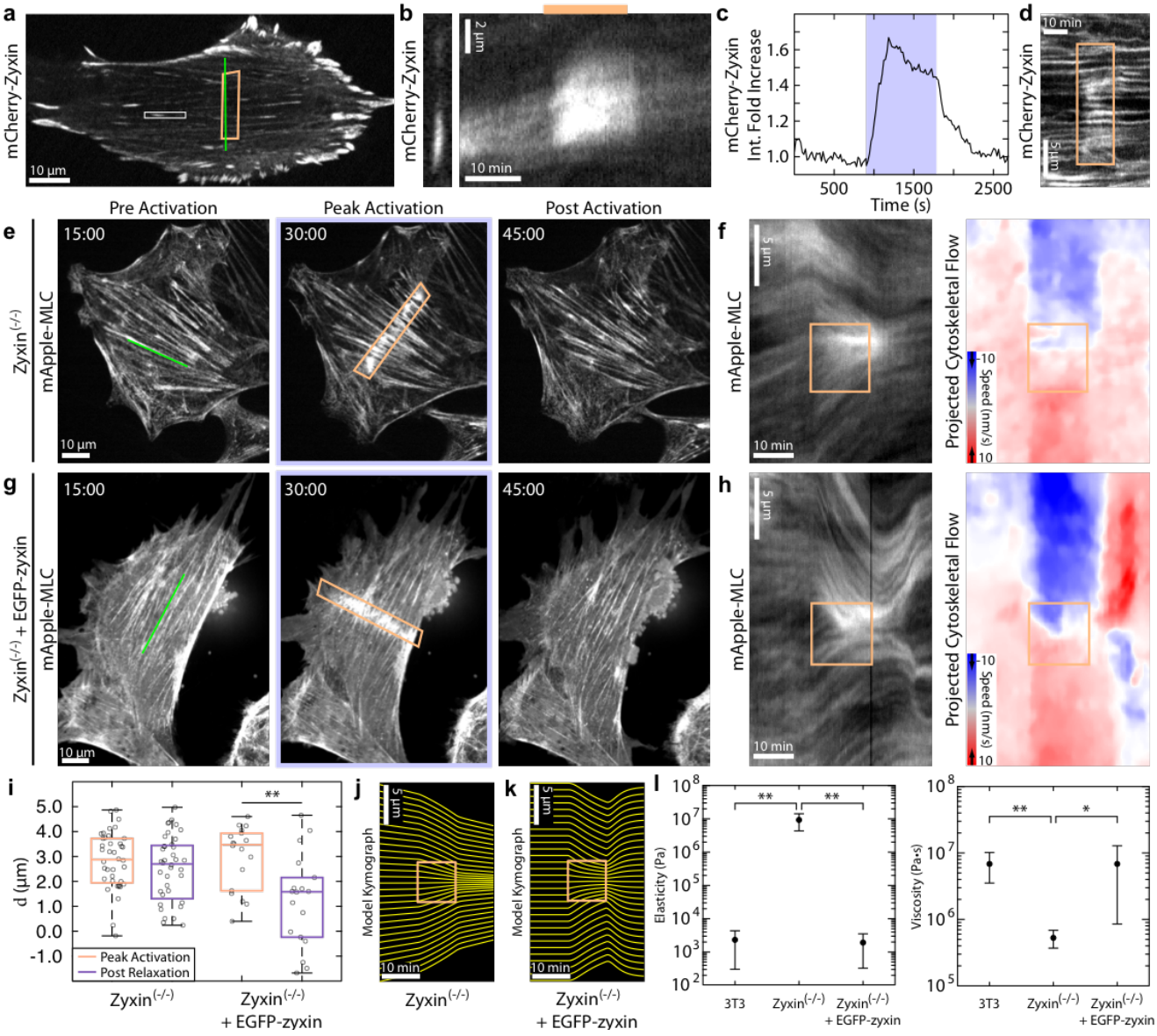

820

821

822 **Figure 6**

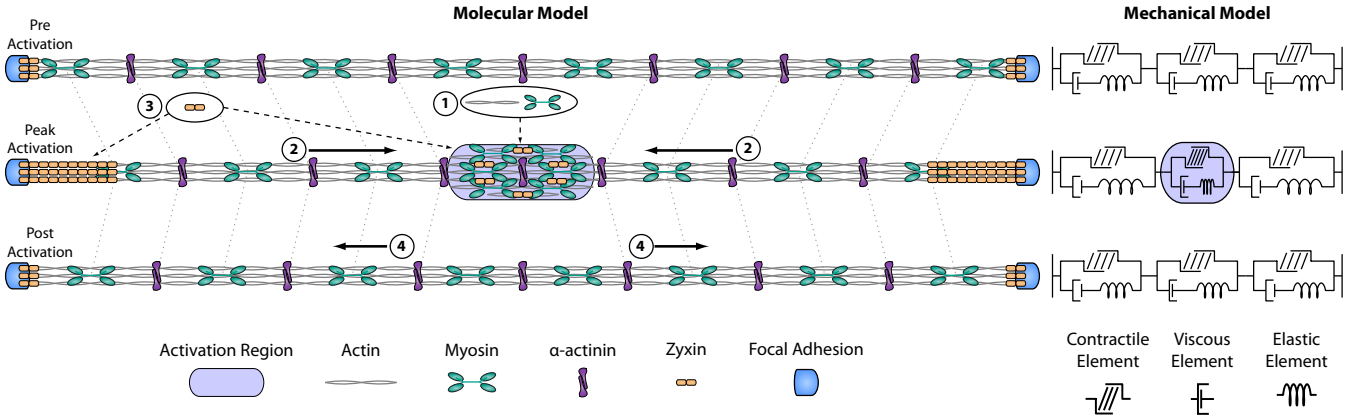

823